CORA Cork Open Research Archive
Cartlann Taighde Oscailte Chorcaí

Title	PCB embedded toroidal inductor for 2MHz point-of-load converter
Authors	Murphy, Ruaidhrí;Pavlovic, Zoran;McCloskey, Paul;O'Mathuna, Cian;O'Driscoll, Séamus;Weidinger, Gerald
Publication date	2020-05-21
Original Citation	Murphy, R., Pavlovic, Z., McCloskey, P., O'Mathuna, C., O'Driscoll S. and Weidinger, G. 'PCB embedded toroidal inductor for 2MHz point-of-load converter', CIPS 2020; 11th International Conference on Integrated Power Electronics Systems, Berlin, Germany, 24-26 March, pp. 280-285. Available at: https://ieeexplore.ieee.org/abstract/document/9097695 (Accessed: 20 August 2021)
Type of publication	Conference item
Link to publisher's version	https://ieeexplore.ieee.org/abstract/document/9097695, https://www.vde-verlag.de/proceedings-de/455225049.html
Rights	© 2020, VDE Verlag. All rights reserved.
Download date	2026-11-16 09:56:22
Item downloaded from	https://hdl.handle.net/10468/11762



UCC
University College Cork, Ireland
Coláiste na hOllscoile Corcaigh

PCB Embedded Toroidal Inductor for 2MHz Point-of-Load Converter

Ruaidhrí Murphy[1], Zoran Pavlovic[1], Paul McCloskey[1], Cian Ó Mathúna[1], Séamus O'Driscoll[1]
[1]Tyndall National Institute, University College Cork, Ireland
Gerald Weidinger[2]
[2]AT&S Austria Technologie & Systemtechnik Aktiengesellschaft

Abstract

Increasing switching frequency, enabled by advances in discrete silicon switches, monolithic CMOS/LDMOS switching bridges and GaN HEMTs, have resulted in a lower inductance requirement for the DC-DC power converter. High density, high efficiency magnetic materials are required to support the increasing power semiconductor switching frequencies. Advanced packaging technologies allow magnetic devices to be integrated within the package substrate of the application Printed Circuit Board (PCB). This paper provides an overview of the magnetic core embedding process technology and a procedure to characterise the magnetic material after its co-processing during the PCB manufacturing process.

1 Introduction

Power conversion for point-of-load (POL) application in power-system-in-package (PwrSiP) format could benefit greatly from the integration of the inductive device in the package substrate. The inductor is typically the largest space consuming discrete component in a POL converter and our goal is to embed it under the active semiconductor components or capacitors. POL applications require the converter to have a high power density and thermal density and therefore the inductor efficiency should be as high as possible such as greater than 96%.

Magnetic material embedding within a PCB must be automatable and be able to withstand the embedding process, the mechanical stresses and reflow temperatures the PCB will be subjected to. An inadequate device moisture-sensitivity-rating for the device (MSR) and/or coefficient of thermal expansion (CTE) can lead to the failure of the device. CTE mismatch between the magnetic material and the PCB internal layers causes stress on the components.

Once a magnetic material has been mechanically certified for PCB embedding, a characterisation of the embedded magnetic performance is needed in order to perform electrical inductor device design with that material.

It has been demonstrated that the toroidal inductor has a low radiated external field in comparison to solenoid and spiral structures [1]. A lower external field reduces the EMI generated by the device and avoids losses in adjacent copper planes and components.

The device featured in this paper is targeted for use with GaN HEMTs in a 12:1V conversion 2-level buck converter at multi-MHz. Embeddable candidate commercially available magnetic materials were selected to be explored for use with high volume PCB manufacturing technologies to construct the device.

2 Embedding Magnetic Material inside PCB

Center core embedding (CCE) technology

Center core embedding is a method to embed active and passive components using an adhesive film to fix the position of the component within a cavity in the laminates' core. In this case the embedded component is a magnetic material. These cavities are realized in a FR4 material PCB core using a cutting technology like routing or laser cutting. Then the adhesive film is laminated over the whole PCB core and the magnetic core is assembled into the cavities in the circuits across the PCB panel (Figure 1).

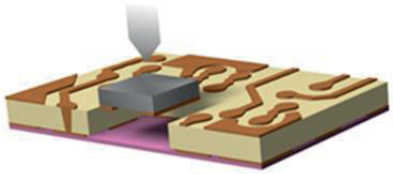


Figure 1 CCE embedded part assembly

A pre-preg is then laminated over the PCB core and the embedded magnetic material in a heat assisted pressing process. The resin will fill the gap around the part to be embedded and fix the position of the magnetic material so that the adhesive carrier film can be removed. A second lamination cycle with a pre-preg used on the other side of the core at higher temperature will then cure the resin completely (Figure 2).

ISBN 978-3-8007-5225-6

© VDE VERLAG GMBH · Berlin · Offenbach
Authorized licensed use limited to: UNIVERSITY COLLEGE CORK. Downloaded on August 20,2021 at 14:25:46 UTC from IEEE Xplore. Restrictions apply.

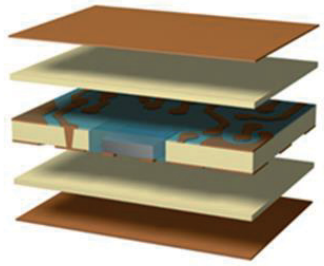


Figure 2 CCE lamination

In the next steps of production, vias are realized from the outer layers of the new 4 layer build-up, down to the copper pads of the embedded part, if necessary, followed by structuring the outer layers to provide a means for unbundling and connecting the contacts of the embedded device (Figure 3). By using the CCE method it is possible to make contact to the embedded device from both sides.

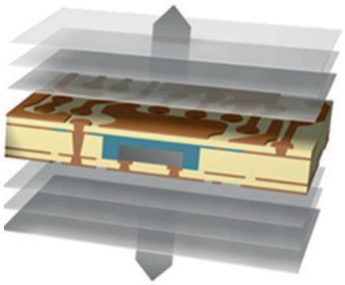


Figure 3 CCE build-up of additional layers

This embedding method allows simultaneous embedding of many devices (actives, passives, switches and controller) and the inductor magnetic core at the central PCB core layer. In addition, using two-step embedding processes it is possible to embed components with different heights. In the case of the magnetic core it is possible to use structuring and the contacting processes to realize windings around the embedded core.

2.1 Magnetic materials

Two types of magnetic material have been used to create test inductor devices for embedding and mechanical qualification and electrical trials. These materials were available in flat sheets suitable for embedding. The magnetic material used:

1. Ferrite particles in resin matrix
2. Metal particles in resin matrix

Ferrite particles in resin matrix material shows good device design flexibility and reliability properties such as CTE control. The small coated particles of this material can be considered a distributed air gap. The ferrite material had to be cured as part of the PCB manufacturing process. Metal particles in resin matrix material gives certain manufacturing advantages. This material is made up of flake particles of metal. The flake type particle promises higher frequency operation because of the small skin depth. The flakes have a high magnetic material fill factor to increase relative permeability

All materials need to be tested for their magnetic properties post processing. The following characteristics are essential for simulations of a design:

- Permeability vs magnetic field strength across frequency.
- Magnetic flux density vs. magnetic field strength curve (Dynamic B-H curve) across frequency.
- Small signal and large signal Q vs magnetic field strength across frequency.

The materials need to be suitable for PCB embedding processes. They must not contain any voids or volatile components (outgassing can occur) and both material and binder must be temperature stable over a standard lead free reflow temperature profile with >260°C peak. All materials have been embedded in a test device and subjected ten times to a standard lead free reflow cycle followed by a cross sectioning test to examine for possible delamination. All materials not passing this test have been excluded from the list of suitable materials.

2.2 PCB design rules

For the test inductor device, a via drill hole-to-hole clearance of 160µm is required on a drill hole minimum diameter is 150µm. An annular ring of 125µm is required. The maximum number of vias which can be placed on the inside of the toroid is:

$$Max\ turn\ count = \frac{2\pi R_{winding_inner_radius}}{via_{\text{hole-to-hole_clearence}}} \qquad (1)$$

where $R_{winding_inner_radius}$ is the inner radius of the winding (see Figure 4).

Minimum line spacing rules versus copper thickness are given in the table below:

Table 1 Minimum line spacing to copper thickness

Copper thickness [µm]	Min. line and space [µm]
0 - 20	50
21 - 25	60
26 - 30	70
31 - 35	75
36 - 45	90
46 - 55	100
56 - 65	125
66 - 75	150
76 - 85	175
86 - 95	200
96 - 105	250

Embedded component thickness can range from 60µm up to 600µm for prototyping. 400µm to 500µm magnetic core thickness proved as a practical compromise for low profile inductor devices.

ISBN 978-3-8007-5225-6

© VDE VERLAG GMBH · Berlin · Offenbach
Authorized licensed use limited to: UNIVERSITY COLLEGE CORK. Downloaded on August 20,2021 at 14:25:46 UTC from IEEE Xplore. Restrictions apply.

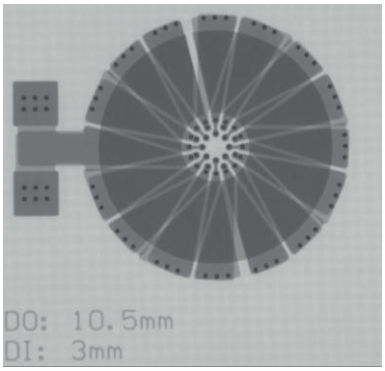


Figure 4 X-ray image of the inductor showing winding turn tilt and vias in the centre of the toroid

3 Device for characterisation of embedded magnetic material

A test device was fabricated using AT&S CCE technology to characterise the embedded magnetic material after fabrication (see Figure 5). The thickness of the magnetic core was 400µm, within the design rule limits.

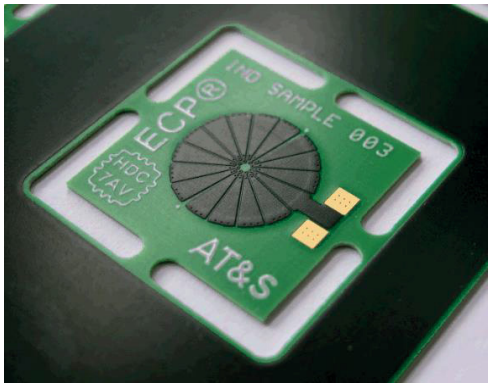


Figure 5 Finished test device inductor

Thin copper layers above and below the core are interconnected with vias creating an enclosed winding structure. High copper density per turn reduces inter turn magnetic field fringing in the device.

3.1 Small signal measurement

The inductor was measured using a HP E4980A LCR meter with a DC bias unit at 2MHz with a small signal amplitude of 10mA.

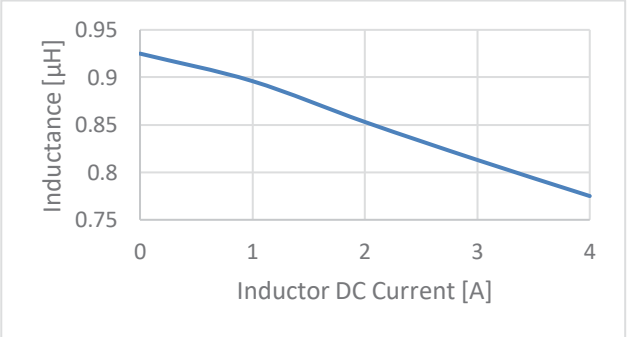


Figure 6 Small signal inductance for the test device with ferrite particles in resin matrix material vs DC current

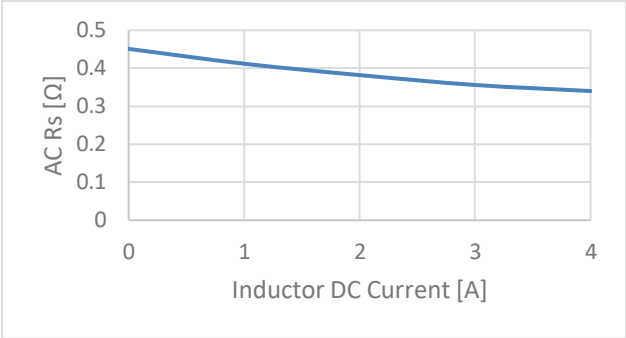


Figure 7 Small signal equivalent AC series resistance for the test device with ferrite particles in resin matrix material (copper and core loss) vs DC current

An inductance of 775nH at 4A was achieved with a small signal resistance of 340mΩ and a small signal Q of 28 for the ferrite particles in resin matrix material device. Inductance and resistance decrease with higher magnetic field strengths.

3.2 Large signal measurement

Large signal testing was undertaken to determine the performance of the inductor under the conditions the material will experience in a converter. A half bridge configuration with a series capacitor which removes the DC component of the square wave excitation was used. This is representative of converter operating conditions.

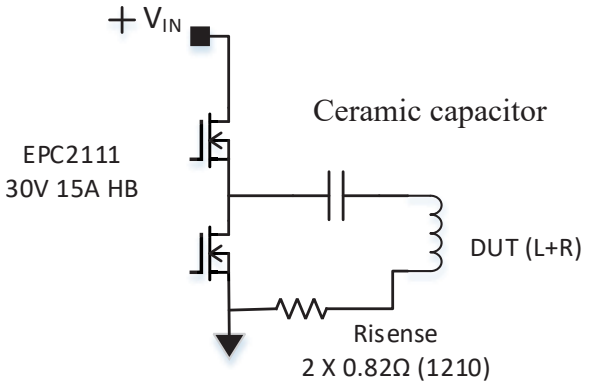


Figure 8 Large signal characterisation circuit (inductor ripple current is similar to a buck family converter)

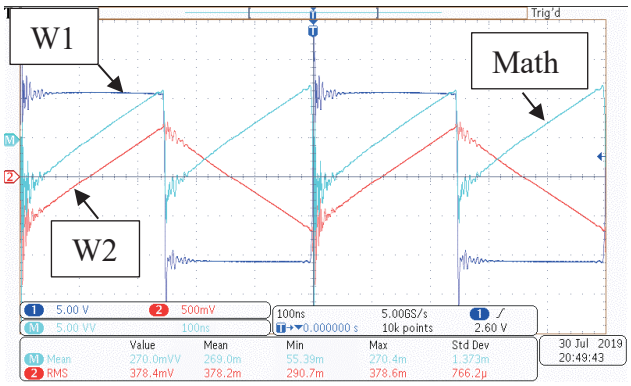


Figure 9 In-converter inductor waveforms at 2MHz (W1: voltage across inductor and sense resistor. W2: voltage across the sense resistor. Math: inductor voltage multiplied by the resistor voltage.)

ISBN 978-3-8007-5225-6

© VDE VERLAG GMBH · Berlin · Offenbach
Authorized licensed use limited to: UNIVERSITY COLLEGE CORK. Downloaded on August 20,2021 at 14:25:46 UTC from IEEE Xplore. Restrictions apply.

$$L = \frac{V_L . d_t}{d_i} = \frac{11 \times 240 \times 10^{-9}}{3.33} = 792nH$$

$$P_{inductor} = \frac{(V_L \times V_{Risense})}{R_{isense}} = (0.271 \div 0.41) = 0.658W$$

Table 2 Large signal results

L @3.3A peak-to-peak	792nH
Rac large signal in-converter equivalent	812mΩ
Q large_signal_in_converter equivalent	12.25

The in-converter equivalent resistance has increased in comparison to the small signal resistance and the inductance is lower than the small signal inductance of 870nH at DC 1.65A peak. The loss experienced by the inductor device in-converter is higher than under small signal conditions due to the triangular flux waveform which has higher order harmonics and no DC bias.

4 Determination of Embedded Magnetic Material Characteristics

The air core inductance and resistance of the copper windings were simulated using finite-element-analysis (FEA) software. The measured small signal inductance and resistance for the test device consists of inductance and resistance caused by the air core and the magnetic material. Removing the air core inductance and resistance isolates the magnetic material measurements. Real permeability was then calculated using the extracted small signal inductance from the test device:

$$L(I) = \int_{Ri}^{Ro} \frac{\mu_0 \mu'(H) H N t_{core}}{I}\, dr \qquad (2)$$

where N is number of turns, μ_0 is permeability of free space, $\mu'(H)$ is relative permeability at H, H is the magnetic field strength, t_{core} is the thickness of the core, L(I) is the inductance at current I, I is current and Ro is the outer radius and Ri is the inner radius of the toroid. Permeability is varying across the core with magnetic field strength from inner to outer radius and therefore a fourth order polynomial is used to model $\mu'(H)$.

$$L(I) = \int_{Ri}^{Ro} \mu_0 \left(a_4 \left(\frac{NI}{2\pi r}\right)^4 \ldots + a_0\right) \frac{N^2}{2\pi r} t\, dr \qquad (3)$$

With sufficient set of data points for inductance vs DC current, the polynomial coefficients can be solved and the permeability known at each magnetic field strength. Imaginary permeability is calculated using the measured AC resistance (representing magnetic core loss) vs the current of the device. The power loss of the magnetic material in a toroidal shape [2]:

$$P_{loss} = \iiint_V \frac{\omega}{2} \mu_0 \mu''(H) H . H^*\, dv \qquad (4)$$

$$P_{loss} = I^2 R_s \qquad (5)$$

$$R_s = \iiint_V \frac{\omega \mu_0 \mu''(\mathrm{H}) H . H^*\, dv}{2I^2} \qquad (6)$$

$$R_s = \int_{Ri}^{Ro} \frac{\omega \mu_0 \mu''(H) N^2\, t 2\pi r\, dr}{4\pi^2 r^2} \qquad (7)$$

$$R_s = \int_{Ri}^{Ro} \frac{\omega \mu_0 (a_4 \left(\frac{NI}{2\pi r}\right)^4 \ldots + a_0) N^2\, t_{core}\, dr}{2\pi r} \qquad (8)$$

where R_s is the equivalent series resistance, μ"(H) is the imaginary permeability at H and ω is angular frequency. The polynomial is used to solve for μ"(H). Figures 10 to 13 detail the results of two different commercial materials for the targeted frequency of 2MHz. A current creates a magnetic field strength at a magnetic path length according to ampere's law.

$$H_{Bias} = \frac{NI_{Bias}}{2\pi r_l} \qquad (9)$$

Where r_l is radius for the magnetic path length l.

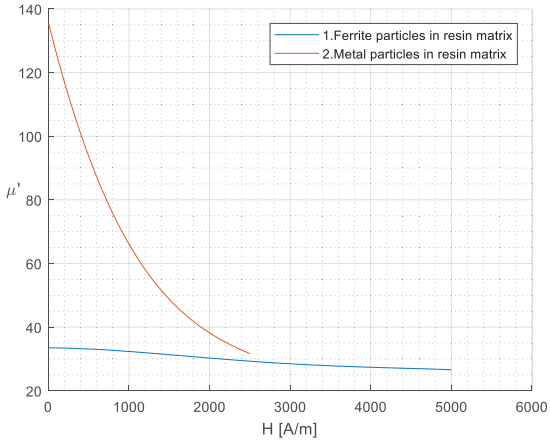


Figure 10 Extracted small signal magnetic material real permeability vs magnetic field strength at 2MHz

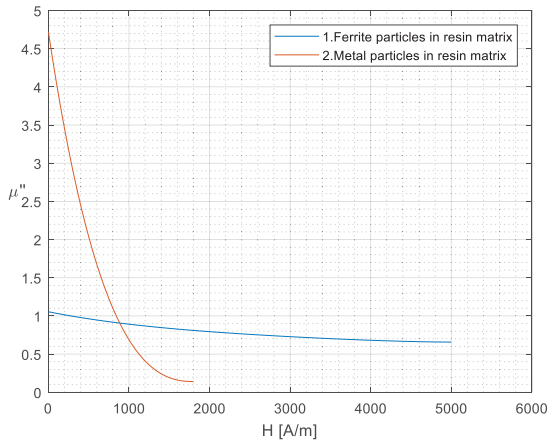


Figure 11 Extracted small signal magnetic material imaginary permeability vs magnetic field strength at 2MHz

Authorized licensed use limited to: UNIVERSITY COLLEGE CORK. Downloaded on August 20,2021 at 14:25:46 UTC from IEEE Xplore. Restrictions apply.

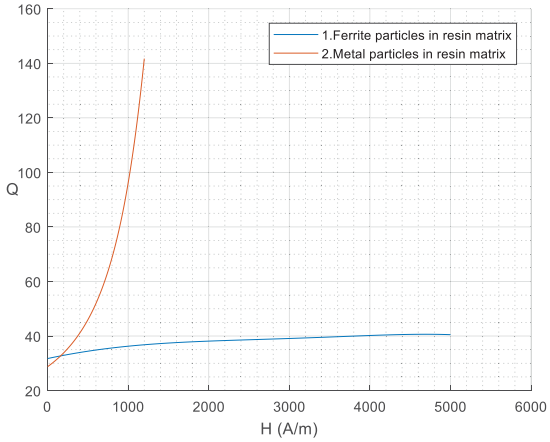


Figure 12 Extracted small signal magnetic material quality factor vs magnetic field strength at 2MHz

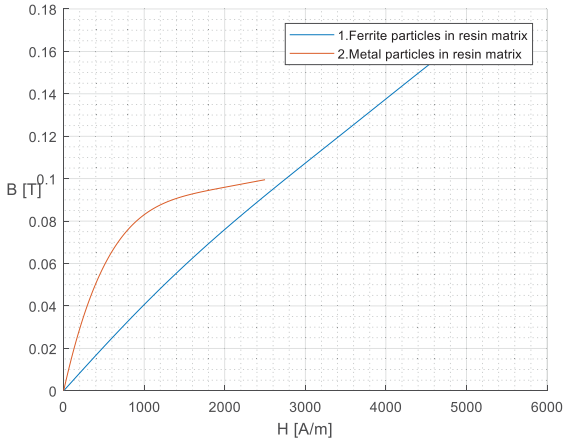


Figure 13 Extracted small signal magnetic material magnetic flux density vs magnetic field strength at 2MHz

The ferrite particle material has a distributed air gap and a lower magnetic material fill factor than the metal particle material resulting in a lower permeability and higher magnetic flux density saturation.

5 Embedded Inductor Electrical Design Process

To validate the magnetic material characterisation an electrical design of the device for the ferrite particles-in-resin matrix material was undertaken. The measured device was matched analytically and with the FEA simulator using the small signal material properties. Large signal material properties could be used to match the device's in-converter performance

Table 3 Test device physical data

Turns	16
Magnetic core outer radius (Ro)	5.25mm
Magnetic core inner radius (Ri)	1.5mm
Magnetic core thickness (t)	400µm
Copper thickness (tcu)	35µm

5.1 Analytical calculation of test inductor

A major component of inductor loss is due to the DC resistance. The analytical equation for DC resistance of a toroidal embedded inductor is [3]:

$$Rdc = \left(\frac{N^2\rho_{cu}}{\pi t_{cu}} \ln\frac{Ro}{Ri} \times F_{tilt}\right) \tag{10}$$

F_{tilt} is the tilt factor to account for the increase in resistance due to the tilt of individual turns. DC resistance is a function of the square of the number of turns (N) on the inductor, the toroid aspect ratio (Ro:Ri) and the copper thickness t_{cu}. Vias are used to connect individual turns, between top and bottom copper layers, also contribute resistance [4]:

$$Rdc = \left(\frac{N^2\rho_{cu}}{\pi t_{cu}} \ln\frac{Ro}{Ri} \times F_{tilt}\right) + \left(N \times (\mathrm{R}_{\mathrm{inner}_{via}} + R_{outer_{via}})\right) \tag{11}$$

It will now be shown that inductance also scales to the square of N and the aspect ratio:

$$L = \frac{N\int_{R1}^{R2} BA_{core}}{I} \tag{12}$$

$$L = \mu_0\mu_r \frac{N^2}{2\pi} t_{core} \ln\frac{Ro}{Ri} \tag{13}$$

Using reluctances the inductance of a device with a magnetic core and airgap is:

$$L = \frac{N^2}{\mathcal{R}_C + \mathcal{R}_g} \tag{14}$$

The magnetic reluctance can be expressed as [5]:

$$\mathcal{R}_C = \frac{l_{core}}{\mu_0\mu_r A_{core}} \tag{15}$$

The reluctance of an air gap can be expressed as:

$$\mathcal{R}_g = \frac{l_{gap}}{\mu_0 A_{core} F_f} \tag{16}$$

where l_{gap} is the length of the air gap and F_f is the air gap flux fringe factor [6]. The air gap reduces the magnetic field strength across the magnetic core to prevent saturation however the inductance of the device will normally decrease.

The analytical model does not take into account the skin effect in the copper windings and fringing flux eddy current loss.

ISBN 978-3-8007-5225-6

© VDE VERLAG GMBH · Berlin · Offenbach
Authorized licensed use limited to: UNIVERSITY COLLEGE CORK. Downloaded on August 20,2021 at 14:25:46 UTC from IEEE Xplore. Restrictions apply.

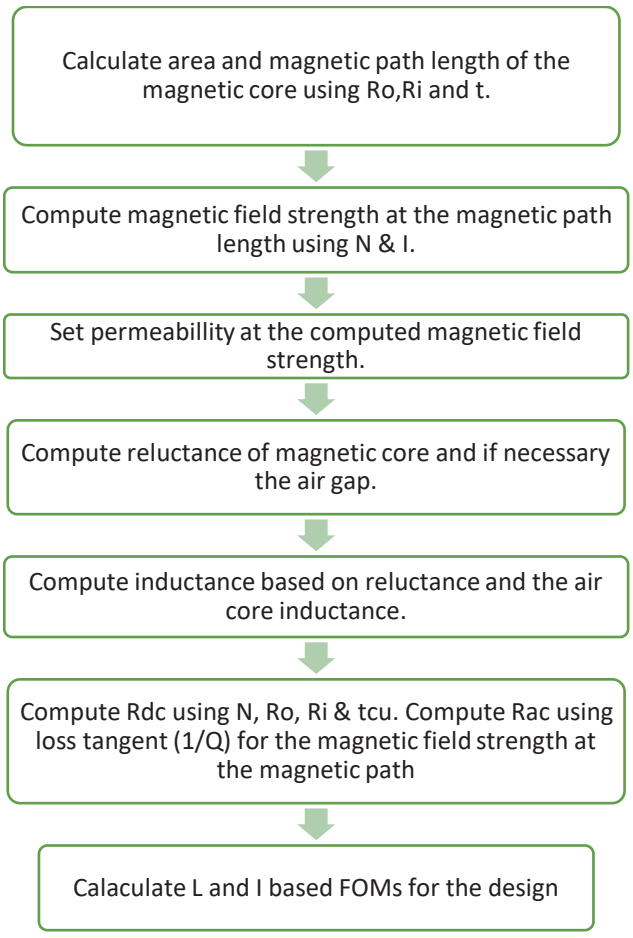


Figure 14 Analytical calculation of test device inductor

5.2 Finite element analysis (FEA)

The design is verified using finite element analysis (FEA). Ansys Maxwell 3D is the software used. The toroid was drawn according to the physical data (see table 3). An eddy-current solver running at 2MHz calculated the inductance and resistance of the device.

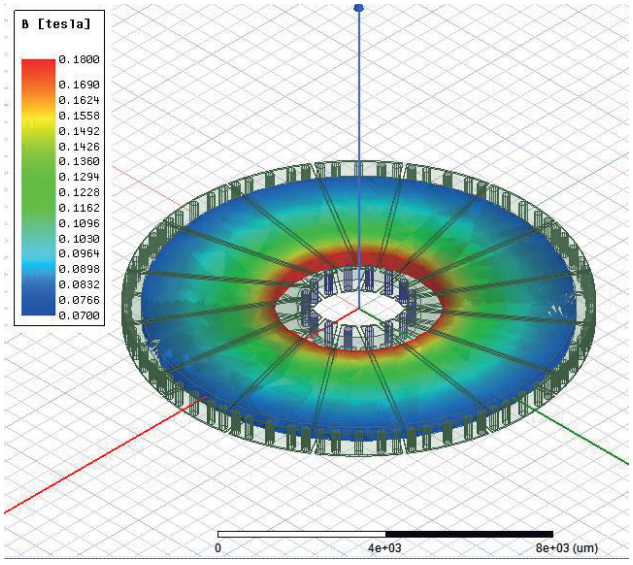


Figure 15 FEA simulation of design showing magnetic flux density varying from 0.070T to 0.180T.

The magnetic material small signal B-H characteristics and a single loss tangent value corresponding to the magnetic field strength at the middle of the magnetic core at 2MHz were input to the simulator. The magnetic flux density is plotted across the core in the FEA simulator. A peak flux density occurs at the innermost part of the toroid at 0.180T.

Table 4 Analytical and FEA results

	Analytical	FEA	Small Signal Measured
L @ 4A	771nH	783nH	775nH
Rdc	54mΩ	76mΩ	66mΩ
R @ 2MHz	294mΩ	320mΩ	340mΩ

6 Conclusions

A test inductor device has been manufactured using AT&S CCE technology and the embedded magnetic material characterised. The test inductor has an inductance density of 9nH/mm^2, an inductance to DC resistance ratio of 11.7nH/mΩ, an inductance to AC resistance ratio of 2.3nH/mΩ and small signal Q of 28.6 at 2MHz. The embedding of the inductor allows other components to use the space available on the top and bottom sides of the board. This device can be fabricated in an automated production facility. The spacing limits of the technology restrict the number of turns that can be realised. A racetrack layout could increase the maximum number of turns.

7 Acknowledgement

This research is part of the EU project GaNonCMOS.

8 References

[1] M. Madsen, A. Knott, M. A. E. Andersen and A. P. Mynster, "Printed circuit board embedded inductors for very high frequency Switch-Mode Power Supplies," 2013 IEEE ECCE Asia Downunder, Melbourne, VIC, 2013, pp. 1071-1078.

[2] R.F. Harrington, "Time-Harmonic Electromagnetic Fields", 1961 ISBN: 9780470546710

[3] Y. E. Zhang and S. R. Sanders, "Design, manufacture and application of in-board magnetic devices," The 4th International Power Electronics and Motion Control Conference, 2004. IPEMC 2004., Xi'an, 2004, pp. 1791-1798 Vol.3.

[4] M. Biglarbegian, "Design and evaluation of high current PCB embedded inductor for high frequency inverters," 2016 IEEE Applied Power Electronics Conference and Exposition (APEC), Long Beach, CA, 2016, pp. 2998-3003.

[5] A. F. Witulski, "Introduction to modeling of transformers and coupled inductors," in IEEE Transactions on Power Electronics, vol. 10, no. 3, pp. 349-357, May 1995.

[6] TRANSFORMER AND INDUCTOR DESIGN HANDBOOK Third Edition, Revised and Expanded COLONEL WM. T. MCLYMAN

Authorized licensed use limited to: UNIVERSITY COLLEGE CORK. Downloaded on August 20,2021 at 14:25:46 UTC from IEEE Xplore. Restrictions apply.